

The Brainbox - a tool to facilitate correlation of brain magnetic resonance imaging features to histopathology

Wolfgang Faigle^{1*}, Marco Piccirelli², Tibor Hortobágyi³, Karl Frontzek^{3,†}, Amelia Elaine Cannon²,
Wolfgang Emanuel Zürcher², Tobias Granberg⁴, Zsolt Kulcsar², Thomas Ludersdorfer¹, Katrin B. M.
Frauenknecht^{5,6}, Regina Reimann³, Benjamin Victor Ineichen^{2,7}

Affiliations

¹ Neuroimmunology and MS Research Section, Neurology Clinic, University Zurich, University Hospital Zurich, Zurich, Switzerland.

² Department of Neuroradiology, Clinical Neuroscience Center, University Hospital Zurich, University of Zurich, Zurich, Switzerland.

³ Institute of Neuropathology, University of Zurich, Zurich, Switzerland.

⁴ Department of Neuroradiology, Karolinska University Hospital, Stockholm, Sweden.

⁵ Luxembourg Center of Neuropathology (LCNP), Laboratoire National de Santé, 3555 Dudelange, Luxembourg.

⁶ National Center of Pathology (NCP), Laboratoire National de Santé, Dudelange, Luxembourg.

⁷ Center for Reproducible Science, University of Zurich, Zurich, Switzerland.

† Current affiliation: Queen Square Brain Bank for Neurological Disorders, UCL Queen Square Institute of Neurology, London, United Kingdom.

*Current address: Institut Curie, PSL University, INSERM U932, Immunity and Cancer, 75005 Paris, France.

Correspondence to:

Benjamin V. Ineichen, MD, PhD

benjamin.ineichen@uzh.ch

Hirschengraben 84

8001 Zürich

Switzerland

Correspondence may also be sent to:

Wolfgang Faigle, PhD

wolfgang.faigle@curie.fr

Institut Curie

75005 Paris

France

<https://mc.manuscriptcentral.com/braincom>

Short title

The Brainbox to correlate MRI-histology

Abstract

Magnetic resonance imaging (MRI) has limitations in identifying underlying tissue pathology, which is relevant for neurological diseases such as multiple sclerosis, stroke, or brain tumours. However, there are no standardized methods for correlating MRI features with histopathology. Thus, here we aimed to develop and validate a tool that can facilitate the correlation of brain MRI features to corresponding histopathology. For this, we designed the Brainbox, a waterproof and MRI-compatible 3D printed container with an integrated 3D coordinate system. We used the Brainbox to acquire post-mortem *ex vivo* MRI of eight human brains, fresh and formalin-fixed, and correlated focal imaging features to histopathology using the built-in 3D coordinate system. With its built-in 3D coordinate system, the Brainbox allowed correlation of MRI features to corresponding tissue substrates. The Brainbox was used to correlate different MR image features of interest to the respective tissue substrate, including normal anatomical structures such as the hippocampus or perivascular spaces, as well as a lacunar stroke. Brain volume decreased upon fixation by 7% ($p = 0.01$). The Brainbox enabled degassing of specimens prior to scanning, reducing susceptibility artifacts, and minimizing bulk motion during scanning. In conclusion, our proof-of-principle experiments demonstrate the usability of the Brainbox, which can contribute to improving the specificity of MRI and the standardization of the correlation between post-mortem *ex vivo* human brain MRI and histopathology. Brainboxes are available upon request from our institution.

Key words

Neuroimaging, magnetic resonance imaging, histopathology, correlation, multiple sclerosis

Introduction

Brain magnetic resonance imaging (MRI) is a sensitive tool that can detect even the smallest pathological changes, making it a critical tool for the diagnosis and monitoring of various neurological diseases such as multiple sclerosis (MS), stroke, and brain tumours. However, conventional MRI has limited specificity for ongoing tissue pathology. This applies particularly to neurological diseases with

1
2
3 a complex underlying tissue pathology like MS ¹, including breakdown of the blood-brain barrier
4 (BBB), infiltration of macrophages, T and B lymphocytes, destruction of myelin sheaths, microglial
5 and astrocytic activation, and neurodegeneration ^{2,3}. In contrast to this heterogenous pathology, MS
6 lesions mostly present homogeneously as hyperintense on T2-weighted images and hypointense on T1-
7 weighted images ⁴.

8
9
10
11
12 To gain a more comprehensive understanding of the relationship between imaging features and
13 corresponding pathologic tissue alterations, there has been an increasing use of the approach of
14 acquiring both MRI and histopathology within the same tissue ⁵. This approach allows for the
15 correlation of imaging features with the corresponding tissue pathology, e.g., for MS ⁶⁻⁸, cerebral
16 microbleeds ^{9,10}, stroke ¹¹, brain tumours ¹², but also for anatomical features such as the entorhinal cortex
17 ¹³. In addition, this allows the correlation of dedicated MRI sequences to key brain metabolites such as
18 iron ^{14,15}. Large endeavours such as the Digital Brain Bank are taking up on this opportunity ⁵.

19
20
21
22
23
24 The standard approach to assess the tissue signature of MRI features is manual correlation ¹⁶⁻¹⁸, which
25 can be highly labour-intensive and is prone to intra/inter-rater variability and inaccuracy. A more
26 standardized and accurate approach is needed to facilitate the process of MRI-histopathology
27 correlation, particularly when correlating small imaging features such as enlarged perivascular spaces
28 ¹⁹⁻²¹ or MS lesions to their tissue signature in a 3D imaging volume.

29
30
31
32
33 Therefore, the objective of this study was to develop and validate a tool that facilitates MRI-
34 histopathology correlation, enabling standardized pipelines for correlating imaging features with
35 corresponding pathology at the tissue level.

36 37 38 39 40 41 42 **Materials and Methods**

43 44 45 **Development of the Brainbox**

46 Over a period of around four years, the Brainbox was developed as a compoundable, waterproof, and
47 fully MRI-compatible container with an integrated 3D coordinate system. In this paper, we present the
48 most recent fit-for-purpose iteration which is now used in our clinical routine (**Figure 1**). Of note, we
49 also include data from the second most recent Brainbox version with a slightly different 3D coordinate
50 system.

51
52
53
54
55 To create the Brainbox, a mould was designed based on an averaged brain model, which was inferred
56 from 109 full brain *in vivo* MRI scans, expanded to each side by 1.5 cm. The box was then printed using
57 an HP Jet Fusion 4200 3D printer with a nylon powder print component (HP PA12). Each axially
58 oriented element of the Brainbox was imprinted with a 3D coordinate system to facilitate precise spatial
59
60

orientation of the brain during and after imaging for correlation with histology features. Note that the imprinted coordinate system allows unequivocal identification of the right and left, anterior and posterior as well as inferior and superior side of the brain and is thus compatible with different spatial axes nomenclatures such as RAS or LAS in the MRI viewer.

Two lids were manufactured for the Brainbox, one with an MR-compatible standard lid and another with a (non-MRI compatible) vacuum valve for degassing the specimen prior to imaging. The latter lid is replaced with the standard lid after degassing and prior to MR imaging. Degassing was performed using a benchtop laboratory aspirator system connected to the Brainbox via the vacuum valve and with a vacuum strength of -0.75 bar.

Human brains and ethical approval

All experimental procedures involving human tissue have been approved by the local ethics board (Cantonal Ethics Committee Zurich, No. 2014-0243) and informed consent has been given by all subjects or their next of kins. Human brains were placed in the Brainbox after autopsy and immersed in PBS. The brains were scanned within 3-10 hours after immersion in PBS. Postmortem intervals ranged from death to brain retrieval between 2 and 18 hours, and from autopsy to scanning between 2 and 18 hours (**Table 1**). After imaging, PBS in the Brainbox was replaced by 4% formaldehyde solution to fixate the tissue for at least 2 weeks. The brain was then scanned a second time to enable a direct comparison of fresh and formaldehyde-fixed brains. Subsequently, the brains were subjected to autopsy by a neuropathologist. The brains were cut in axial slabs guided by the grooves imprinted on the axial Brainbox elements. Selected imaging features were identified on post- (and if available pre-) mortem MRI scans, and corresponding brain tissue blocks were sampled using a brain knife based on the built-in guidance grooves.

Magnetic resonance imaging

Image acquisition was performed on a 3 Tesla MRI scanner (Magnetom Skyra, Siemens Healthcare, Erlangen, Germany). All MRI images were acquired using a 20-channel head coil for signal reception. The MRI protocol comprised a T1-weighted (T1w) scout sequence for planning, a high-resolution 3D MPRAGE T1w sequence, a 3D high-resolution T2w SPACE sequence, a 3D high-resolution susceptibility-weighted sequence (SWI), and a 3D high-resolution double inversion recovery (DIR) sequence. All images had a nominal resolution of $0.4 \times 0.4 \times 0.7 \text{ mm}^3$ (except the DIR which had a resolution of $0.5 \times 0.5 \times 0.7 \text{ mm}^3$), which was sufficient to correlate even small pathologies like a lacunar stroke. Total scanning time was around 2 hours. The sequence parameters are summarised in **Supplementary Table 1**.

Of note, chemical preservation of post-mortem tissue with aldehyde solutions (e.g., formalin) results in shortened relaxation time constants (T1, T2, and T2*)²². This is particularly important for the

1
2
3 convergence of T1 of gray and white matter, leading to poor contrast with conventional T1w structural
4 sequences ²³.

5
6 MRI volumes of brains before and after formaldehyde fixation were manually segmented on T1-
7 weighted scans using ITK-SNAP ²⁴.

10 11 12 Histopathology

13 Tissue blocks were paraffin-embedded and cut on a microtome into 3 – 5 µm thick sections. For
14 histological characterization of the MRI features, the following antibodies were used: CD68 (DAKO,
15 clone PG-M1, 1:100), and GFAP (Dako, GA52461-2, 1:100). For immunohistochemistry, slides were
16 incubated with PBS before and blocking in PBS/10%BSA for 1 hour at room temperature. Endogenous
17 peroxidase was blocked with 0.3% hydrogen peroxide for 20 min. Slides were incubated with primary
18 antibodies overnight at 4°C. Secondary biotinylated antibody was applied for 1 hour at room
19 temperature followed by the ABC complex reagent (VectorLabs) for one hour. The colour reaction was
20 carried out with “ImpactDAB” (VectorLabs). All counterstainings were done with Hematoxylin. In
21 addition, Luxol Fast Blue (LFB) staining was used to assess myelination, Prussian Blue for hemosiderin,
22 and Elastica van Gieson staining to highlight elastic lamina in vessel walls. Subsequently, slides were
23 dehydrated in ethanol/xylol and mounted using “Entellan” (Merck Millipore). Slides were scanned
24 using a Hamamatsu slide scanner (Hamamatsu Photonics). Corresponding microphotographs of regions
25 of interest were taken using NDP.view2 viewing software.

26 27 28 29 30 31 32 33 34 35 Brainbox MRI-histopathology pipeline

36 During the common case round, both the postmortem MRI findings and histopathology findings are
37 discussed in a multidisciplinary team comprising radiologists, neuropathologists, and forensic
38 pathologists.

39 40 41 42 43 Statistical analysis

44 Statistical analysis was conducted in the R programming environment to compare brain volumes before
45 and after formaldehyde fixation (paired t-test). The Shapiro-Wilk test was used to assess normal
46 distribution of our samples. The correlation of pre- and post-fixation volumes was assessed using
47 Pearson’s correlation coefficient.

Results

Brainbox

The Brainbox consists of two compartments: a watertight tank (outer compartment, **Figure 1A-C**) and an inlet holding the brain (inner compartment or brainholder, **Figure 1A, E, and F**). The outer compartment has a size of 23.7 x 20.0 x 19.0 cm, allowing it to fit into a standard 20-channel headcoil from Siemens Skyra. The tank is closed with an MRI-compatible lid using titanium screws and has an aperture at the front end for filling or emptying the tank with fluid. For degassing, a lid with a built-in vacuum valve (not MRI-compatible, **Figure 1D**) is used, which is replaced with a standard MRI-compatible lid before imaging.

The brainholder is composed of 16 stackable elements arranged in axial orientation (**Figure 1A, E, and F**), and each element has a height/thickness of 15 mm, with varying length and width (15.9-19.6 cm and 10.5-14.5 cm **Figure 1G**). The brainholder has a 3D coordinate system with the Z coordinate indicated using roman letters and the X and Y coordinates using countable indents on the outer surface of the brainholder (**Figure 1G**). Each layer is divided into 30-72 quadrants with guidance axes, defining individual brain subvolumes, which can be selected based on imaging volumes of interest. The quadrants have a minimum size of 1.5-2.0 cm, making the excised brain blocks compatible with standard microscope slides. The brainholder can be inserted and removed from the tank using a belt and buckle (**Figure 1B**).

Magnetic resonance imaging

The study included the scanning of eight human brains using the Brainbox (**Table 1**). The imprinted 3D coordinate system on the Brainbox allowed the identification of volumes of interest for subsequent correlation to histopathology (**Figure 2A**).

Whole-brain MRI employing the Brainbox enabled visualisation of pathology such as deep white matter T2w-hyperintensities in the parietooccipital lobes in a patient with X-linked adrenoleukodystrophy (X-ALD, **Figure 2B**) or a patient with middle cerebral artery stroke (**Figure 2D**), similar to the exhibited pathology in premortem MRI (**Figure 2C and F**, respectively). The stroke, represented by T2w hyperintensity, was equally well visible in fresh and fixed brain tissue (**Figure 2D and E**). The Brainbox was also used to acquire a high-resolution MRI from a COVID-19 donor brain (**Figure 3**).

In addition, the Brainbox was able to visualize more discreet and/or confined imaging pathology such as enlarged perivascular spaces in the basal ganglia (**Figure 2G**) or lacunar strokes (**Figure 2H**), similar to the premortem MRI (**Figure J and K**, respectively).

Whole brains show mean volume loss of 7% (standard deviation, \pm SD 1%) upon fixation in formaldehyde (fresh: 1200 ml \pm SD 69 ml; fixed: 1114 ml \pm SD 47 ml, paired t-test: $p = 0.01$, 6 brains included in the analysis, **Table 1**) (**Figure 2I and L**, respectively). There was a high correlation between pre- and post-fixation brains volumes (Pearson's correlation coefficient: 0.64, $p < 0.01$).

1
2
3 We encountered three issues while performing imaging in the Brainbox. (1) The first problem was the
4 presence of air bubbles, which can interfere with the image quality in imaging sequences that are
5 vulnerable to susceptibility artifacts such as T2*w imaging or SWI. Although degassing helped remove
6 most of the air bubbles at the brain surface, it was sometimes necessary to puncture the ventricles using
7 a cannula to release air from the ventricular system. (2) The second issue we encountered was heating
8 of the tissue/imaging medium during imaging. However, we were able to minimize this problem as our
9 imaging protocol did not result in significant heating of the tissue, resulting in less than 1 °C of tissue
10 heating. (3) The third issue we encountered was ribbon-shaped boundary artifacts that could occur when
11 the brain underwent relatively short fixation prior to imaging. This artifact resulted in a ribbon-shaped
12 boundary in signal intensity at the grey-white matter junction.
13
14
15
16
17
18
19
20

21 Correlating MRI features to histopathology/-morphology

22 The postmortem MRI scans of the brains were used to identify volumes of interest for correlation of
23 imaging features to their corresponding histopathology. A total of 12 pathomorphological features were
24 correlated, including deep white matter hyperintensities in X-ALD (x3), enlarged perivascular spaces
25 (EPVS) in the basal ganglia (x3), cerebellar microbleeds (x2), hippocampi (x2), a lacunar stroke in the
26 thalamus/basal ganglia (x1), and an unclear vascular malformation (x1).
27
28
29

30 With its 3D coordinate system, the Brainbox enabled accurate correlation of imaging features to
31 histopathology. This is demonstrated by two concrete examples of MRI-histopathology correlation: (1)
32 A T1w hypointense ovoid lesion (2 x 3 mm) in the right internal capsule most likely representing an
33 enlarged perivascular space or a chronic lacunar stroke (**Figure 4A**). This MRI finding was defined
34 using the 3D coordinate system of the Brainbox (**Figure 4A**). Subsequently, respective coordinates
35 were identified on the Brainbox by disassembling the axially arranged elements until the eligible Z
36 coordinate was located. Using the axially oriented guidance cue of the Brainbox, the brain was dissected
37 in axial direction using a brain knife (**Figure 4B**). With this, the volume of interest became apparent
38 within the brain. Then, the corresponding guidance grooves in X and Y direction were used to dissect
39 the brain tissue block of interest (**Figure 4C**). These brain blocks were then histopathologically
40 processed. Analysis of respective tissue sections showed a focal tissue defect on the Haematoxylin and
41 Eosin staining, a finding consistent with a lacunar stroke (**Figure 4D**). (2) By employing a similar
42 approach as for the lacunar stroke, we used the Brainbox during autopsy workup of a case from the
43 forensic medicine: We correlated an unclear MRI lesion with susceptibility artifacts in the right angular
44 gyrus (**Figure 4E-G**), likely responsible for a fatal generalized seizure. The lesion was identified in the
45 brain using the 3D coordinate system of the Brainbox (**Figure 4H**). The histopathological workup of
46 corresponding brain tissue blocks showed abnormal blood vessels with cavernous dilatations and
47 irregularly thickened walls consistent with a cavernous haemangioma surrounded by reactive gliosis
48 (**Figure 4I-M**).
49
50
51
52
53
54
55
56
57
58
59
60

1
2
3 During the common case round, both the postmortem MRI findings and histopathology findings are
4 discussed in a multidisciplinary team comprising radiologists, neuropathologists, and forensic
5 pathologists. The pipeline is shown in **Figure 5**. This collaborative approach has improved the accuracy
6 of diagnoses and facilitated the identification of findings that might have been missed by either
7 department alone, for example a cerebellar bleeding or an unclear lesion in the angular gyrus (**Figure**
8 **4E-M**).
9
10
11
12
13
14
15
16

17 Discussion

18 Main findings

19 We herein introduce the Brainbox, a tool that facilitates the correlation of post-mortem *ex vivo* MRI and
20 histopathology of human brains. Its 3D coordinate system enabled unequivocal identification of MRI
21 features of interest and correlation to corresponding tissue features. The Brainbox minimized
22 susceptibility artifacts and bulk motion during scanning. The tool has been validated in eight human
23 brains. The Brainbox has facilitated collaboration between the departments of neuroradiology,
24 neuropathology and forensic medicine through a common case round.
25
26
27
28
29
30
31

32 Findings in the context of existing evidence

33 *Ex vivo* imaging studies are commonly done on brain slices or hemispheres. However, imaging the
34 whole brain has several advantages, among them fewer artifacts (e.g., air bubbles and distortion edges)
35 and reduced total scan time for covering the whole brain. However, most importantly, whole-brain
36 imaging preserves landmarks for radiologic interpretation which is especially important for exploratory
37 imaging or examining small focal and more diffuse neuropathologic features. These reasons render
38 whole-brain imaging the most practical approach for a clinical applications²⁵. Moreover, whole-brain
39 imaging is essential for detecting subtle pathology along white matter tracts with advanced techniques
40 such as tractography. With this, we have established a collaboration with the neuropathology and
41 forensic medicine at our hospital for work-up of cases using the Brainbox in clinical rounds.
42
43
44
45
46
47

48 Commonly faced problems during *ex vivo* imaging are air bubbles and (bulk) motion of the brain within
49 the container during scanning caused by buoyancy and/or vibration by certain MRI sequences. The
50 presence of air bubbles can interfere with the image quality in imaging sequences that are vulnerable to
51 susceptibility artifacts such as T2*w imaging or SWI. Although degassing helped remove most of the
52 air bubbles at the brain surface, it was sometimes necessary to puncture the ventricles using a cannula
53 to release air from the ventricular system. Other dedicated approaches to minimize susceptibility
54 artifacts by removing air bubbles from the specimen have been developed^{26,27}. Also, bulk motion was
55 reduced by our Brainbox by serving as a rigid scaffold holding the brain during scanning. Other
56
57
58
59
60

1
2
3 solutions mitigating bulk motion have been proposed, , e.g., by a Plexiglas container which minimizes
4 bulk motion of the brain during scanning ²⁸. We encountered additional challenges while acquiring MR
5 images using the Brainbox: (1) Heating of the tissue/imaging medium during imaging. We were able to
6 minimize this problem as our imaging protocol did not result in significant heating of the tissue,
7 resulting in less than 1 °C of heating; and (2) Ribbon-shaped boundary artifacts that occurred when the
8 brain was subjected to a relatively short fixation period prior to imaging. This artifact resulted in a
9 ribbon-shaped boundary in signal intensity at the grey-white matter junction. Note that immersion
10 fixation can also lead to gradients in fixation quality regardless of fixation time. This is because more
11 superficial brain regions undergo superior tissue preservation compared to deeper brain regions ²⁹.

12
13
14 Other methods for correlating MRI features to the tissue substrate have been developed. Lasserre and
15 colleagues have introduced a 3D-printed mold mounting a whole brain (or a medial temporal lobe) and
16 with interactively placeable guiding indents for sectioning ^{30,31}. Another approach has been developed
17 by Absinta/Guy and colleagues: an individualized, 3D printed cutting box for human ³² or marmoset
18 brains ³³. This method enables monoplanar sectioning of the brain subsequently to postmortem imaging
19 to improve alignment of post-mortem MRI and autopsy brain slabs. Although these approaches are
20 undoubtedly valuable, they are employed after MRI acquisition. In contrast, the Brainbox contains the
21 brain during the entire imaging session as well as the subsequent brain sectioning which alleviates
22 correlation of MRI features to histopathology. With this, the Brainbox can also be used for longterm
23 storage and transport of a whole human brain. It enables time savings in a similar range like published
24 devices ³², i.e., around 2 hours versus 10 – 15 hours for manual correlation. Of note, while it is
25 recommended to preserve samples under appropriate conditions to maintain their integrity, short-term
26 storage at room temperature for neuroimaging in the Brainbox may have minimal impact on commonly
27 used “omics” analyses ^{34,35}.

28
29
30 Post-mortem MRI is an intermediate step for understanding the pathologic basis for MRI signal
31 changes. Yet care should be taken when inferring findings from *ex vivo* histopathology correlation to
32 the *in vivo* paradigm. Findings from a unique case report acquiring ante-mortem and *in situ* post-mortem
33 MRI within only a 4 day interval suggested that brain volume, particularly in the white matter, can
34 substantially increase upon death ³⁶. Additional alterations are entailed by tissue processing prior to
35 autopsy, mostly by formaldehyde-based fixation agents. Such fixation agents change tissue T1 and, to
36 a lesser degree, T2 by decreasing the difference in water mobility between grey and white matter ^{22,37-}
37 ⁴². Early decline in T1 during fixation can lead to convergence of T1 in both grey and white matter ⁴³
38 resulting in poorer grey-white matter contrast or even reversal of relative signal intensities between grey
39 and white matter in T1w sequences ^{23,28,44}. Stable changes of T1 and T2 can be expected after 3 – 4
40 weeks for brain tissue samples and a few months for whole brains ⁴³. Based on this paradigm, dedicated
41 MRI sequences such as spin (proton) density-weighted protocols ²⁸ or steady-state based sequences (e.g.
42 SSFP or TrueFISP) can be advantageous for *ex vivo* MRI ⁷. Of note, long post-mortem intervals can be
43 a confounding factor because they can be associated with tissue decomposition ^{45,46}.

1
2
3 For most clinical scenarios where our Brainbox could be employed, a qualitative correlation of MRI to
4 histopathology will be sufficient. However, certain research questions might require a more accurate
5 correlation of these two domains. In such a case, the histologically stained section can be registered to
6 the *ex vivo* MRI⁴². This process can be challenging due to nonlinear tissue deformation caused by
7 histopathological processing, e.g., tissue sectioning, slide-mounting, air drying, or treatment with
8 solvents⁴⁷⁻⁵². This challenge is particularly relevant for human brain tissue with its highly convoluted
9 cortex. Accurate registration warrants at least a prior affine registration and subsequent deformable
10 alignment^{47,50,53-56}. Blockface images, i.e., images from tissue blocks obtained during sectioning, can
11 facilitate registration by allowing MRI-to-block registration as intermediate step⁴².
12
13
14
15
16
17
18

19 Limitations

20
21 Our Brainbox has some limitations to consider. First, Fomblin, a chemically inert perfluoropolyether
22 fluorocarbon which yields no MRI signal and has a similar magnetic susceptibility to tissue, is
23 commonly used for *ex vivo* MR imaging^{23,32,57}. Currently, the integrated 3D-coordinate system of the
24 Brainbox, which is visualized using the MR signal of an aqueous medium, renders the use of Fomblin
25 suboptimal. However, of note, Fomblin is expensive (>500 US\$ per liter) and leaves oily remnants on
26 the tissue surface which may interfere with subsequent histopathological work-up²⁶. Second, although
27 degassing helped to reduce air bubbles, small remaining air bubbles in the ventricles were commonly
28 encountered. A solution for this has been proposed by Shatil and colleagues, i.e., to inject liquid into
29 the ventricles using a syringe²⁶. Yet neuropathologists should be consulted in advance to avoid
30 interference with the autopsy. Third, the default method for brain sectioning using our Brainbox is the
31 axial/transversal plane which makes the handling of the Brainbox more viable and which is the standard
32 plane for brain MRI scans. This contrasts the coronal sectioning as the standard cutting plane for
33 autopsy. Future iterations of the Brainbox will enable coronal sectioning. Fourth, despite reliable
34 correlation of imaging features to histopathology, our high-resolution MRI scans were anisotropic.
35 Larger scale projects using the Brainbox could implement isotropic MRI scans as regularly done by the
36 Human Connectome Project⁵⁸.
37
38
39
40
41
42
43
44
45
46
47

48 Conclusions

49 The Brainbox cannot only be used for longterm storage and transport of whole human brains but it also
50 facilitates correlation of MRI features to histopathology. With this, our approach embodies the concept
51 that whole-brain *ex vivo* MRI can alleviate and guide neuropathology and thus providing a benchmark
52 for comparison before and after sectioning. This can ultimately benefit specificity of MRI. Brainboxes
53 are available upon request from the corresponding authors.
54
55
56
57
58
59
60

Data availability statement

The MRI data used to investigate our research questions are only available upon special request and in accordance with current legislation since these are sensitive patient data. The R code to conduct the statistical analysis is available upon request from the corresponding author. Brainboxes are available upon request from the corresponding authors.

Acknowledgements

We thank the 3D printing facilities from the University of Zurich (“Additive Manufacturing”) and the Wyss Center Zurich, the joint Translational Center from the ETH and the University of Zurich for supporting our 3D printing of the brainbox. We thank F. Mercury for help with data analysis.

Funding

WF was supported by Swiss National Science Foundation (4078P0_198345). KBMF was supported by a career development award from the Stavros Niarchos Foundation. BVI was supported by the FAN (Förderung des akademischen Nachwuchses) from the UZH Alumni at the University of Zurich, the Swiss Multiple Sclerosis Society, and the Swiss National Science Foundation (P400PM_183884). This project was supported by the University Hospital of Zurich (Innovationspool, to WF and BVI). The funders had no role in study design, data collection and analysis, decision to publish, or preparation of the manuscript.

Competing interests

A patent has been filed for the Brainbox by Wolfgang Faigle, Thomas Ludersdorfer, and Katrin B. M. Frauenknecht. The other authors declare no conflict of interest related to this study.

References

1. Filippi M, Brück W, Chard D, et al. Association between pathological and MRI findings in multiple sclerosis. *The Lancet Neurology*. 2019;18(2):198-210.
2. Filippi M, Rocca MA, Ciccarelli O, et al. MRI criteria for the diagnosis of multiple sclerosis: MAGNIMS consensus guidelines. *The Lancet Neurology*. Mar 2016;15(3):292-303. doi:10.1016/s1474-4422(15)00393-2
3. Lassmann H. Multiple sclerosis pathology. *Cold Spring Harbor perspectives in medicine*. 2018;8(3):a028936.
4. Ineichen BV, Beck ES, Piccirelli M, Reich DS. New Prospects for Ultra-High-Field Magnetic Resonance Imaging in Multiple Sclerosis. *Invest Radiol*. Jun 11 2021;doi:10.1097/rli.0000000000000804
5. Tandler BC, Hanayik T, Ansorge O, et al. The Digital Brain Bank, an open access platform for post-mortem imaging datasets. *eLife*. 2022;11:e73153.
6. Kolb H, Absinta M, Beck ES, et al. 7T MRI differentiates remyelinated from demyelinated multiple sclerosis lesions. *Annals of neurology*. 2021;90(4):612-626.

7. Weigel M, Dechent P, Galbusera R, et al. Imaging multiple sclerosis pathology at 160 μm isotropic resolution by human whole-brain ex vivo magnetic resonance imaging at 3 T. *Scientific reports*. Jul 29 2021;11(1):15491. doi:10.1038/s41598-021-94891-1
8. Jonkman LE, Soriano AL, Amor S, et al. Can MS lesion stages be distinguished with MRI? A postmortem MRI and histopathology study. *Journal of neurology*. 2015;262(4):1074-1080.
9. Jolink WMT, van Veluw SJ, Zwanenburg JJM, et al. Histopathology of Cerebral Microinfarcts and Microbleeds in Spontaneous Intracerebral Hemorrhage. *Transl Stroke Res*. Apr 6 2022;doi:10.1007/s12975-022-01016-5
10. Scherlek AA, Kozberg MG, Nicoll JA, et al. Histopathological correlates of haemorrhagic lesions on ex vivo magnetic resonance imaging in immunized Alzheimer's disease cases. *Brain Communications*. 2022;4(1):fcac021.
11. van Veluw SJ, Arfanakis K, Schneider JA. Neuropathology of Vascular Brain Health: Insights From Ex Vivo Magnetic Resonance Imaging-Histopathology Studies in Cerebral Small Vessel Disease. *Stroke; a journal of cerebral circulation*. Feb 2022;53(2):404-415. doi:10.1161/strokeaha.121.032608
12. Bobholz SA, Lowman AK, Brehler M, et al. Radio-Pathomic Maps of Cell Density Identify Brain Tumor Invasion beyond Traditional MRI-Defined Margins. *AJNR American journal of neuroradiology*. May 2022;43(5):682-688. doi:10.3174/ajnr.A7477
13. Oltmer J, Slepneva N, Llamas Rodriguez J, et al. Quantitative and histologically validated measures of the entorhinal subfields in ex vivo MRI. *Brain Communications*. 2022;4(3):fcac074.
14. Vroegindewij LHP, Wielopolski PA, Boon AJW, et al. MR imaging for the quantitative assessment of brain iron in aceruloplasminemia: A postmortem validation study. *NeuroImage*. Dec 15 2021;245:118752. doi:10.1016/j.neuroimage.2021.118752
15. Langkammer C, Schweser F, Krebs N, et al. Quantitative susceptibility mapping (QSM) as a means to measure brain iron? A post mortem validation study. *NeuroImage*. 2012;62(3):1593-1599.
16. Jonkman LE, Kenkhuis B, Geurts JJ, van de Berg WD. Post-mortem MRI and histopathology in neurologic disease: a translational approach. *Neuroscience Bulletin*. 2019;35(2):229-243.
17. Keren NI, Taheri S, Vazey EM, et al. Histologic validation of locus coeruleus MRI contrast in post-mortem tissue. *NeuroImage*. 2015;113:235-245.
18. Mollink J, Kleinnijenhuis M, van Walsum A-MvC, et al. Evaluating fibre orientation dispersion in white matter: Comparison of diffusion MRI, histology and polarized light imaging. *NeuroImage*. 2017;157:561-574.
19. Haider L, Hametner S, Endmayr V, et al. Post-mortem correlates of Virchow-Robin spaces detected on in vivo MRI. *Journal of cerebral blood flow and metabolism : official journal of the International Society of Cerebral Blood Flow and Metabolism*. May 17 2022;271678x211067455. doi:10.1177/0271678x211067455
20. Ineichen BV, Okar SV, Proulx ST, Engelhardt B, Lassmann H, Reich DS. Perivascular spaces and their role in neuroinflammation. *Neuron*. 2022/11/02/ 2022;110(21):3566-3581. doi:https://doi.org/10.1016/j.neuron.2022.10.024
21. Ineichen BV, Cananau C, Plattén M, et al. Dilated Virchow-Robin spaces are a marker for arterial disease in multiple sclerosis. *EBioMedicine*. 2023;92
22. Birkl C, Langkammer C, Golob-Schwarzl N, et al. Effects of formalin fixation and temperature on MR relaxation times in the human brain. *NMR in biomedicine*. 2016;29(4):458-465.
23. Miller KL, Stagg CJ, Douaud G, et al. Diffusion imaging of whole, post-mortem human brains on a clinical MRI scanner. *NeuroImage*. 2011;57(1):167-181.
24. Yushkevich PA, Gao Y, Gerig G. ITK-SNAP: An interactive tool for semi-automatic segmentation of multi-modality biomedical images. *IEEE*; 2016:3342-3345.
25. Pollanen MS, Woodford N. Virtual autopsy: time for a clinical trial. *Forensic science, medicine, and pathology*. 2013;9(3):427-428.

26. Shatil AS, Matsuda KM, Figley CR. A Method for Whole Brain Ex Vivo Magnetic Resonance Imaging with Minimal Susceptibility Artifacts. *Front Neurol.* 2016;7:208. doi:10.3389/fneur.2016.00208
27. Edlow BL, Mareyam A, Horn A, et al. 7 Tesla MRI of the ex vivo human brain at 100 micron resolution. *Scientific data.* 2019;6(1):1-10.
28. Schumann CM, Buonocore MH, Amaral DG. Magnetic resonance imaging of the post-mortem autistic brain. *J Autism Dev Disord.* Dec 2001;31(6):561-8. doi:10.1023/a:1013294927413
29. Bauer DR, Stevens B, Chafin D, Theiss AP, Otter M. Active monitoring of formaldehyde diffusion into histological tissues with digital acoustic interferometry. *Journal of Medical Imaging.* 2016;3(1):017002-017002.
30. Yushkevich PA, Muñoz López M, Iñiguez de Onzoño Martin MM, et al. Three-dimensional mapping of neurofibrillary tangle burden in the human medial temporal lobe. *Brain : a journal of neurology.* Oct 22 2021;144(9):2784-2797. doi:10.1093/brain/awab262
31. Lasserre J, Lim SA, Wisse L, et al. Optimized extraction of the medial temporal lobe for postmortem MRI based on custom 3D printed molds: Neuroimaging/New imaging methods. *Alzheimer's & Dementia.* 2020;16:e043254.
32. Absinta M, Nair G, Filippi M, et al. Postmortem magnetic resonance imaging to guide the pathologic cut: individualized, 3-dimensionally printed cutting boxes for fixed brains. *Journal of neuropathology and experimental neurology.* Aug 2014;73(8):780-8. doi:10.1097/nen.0000000000000096
33. Guy JR, Sati P, Leibovitch E, Jacobson S, Silva AC, Reich DS. Custom fit 3D-printed brain holders for comparison of histology with MRI in marmosets. *Journal of neuroscience methods.* Jan 15 2016;257:55-63. doi:10.1016/j.jneumeth.2015.09.002
34. Marsh SE, Walker AJ, Kamath T, et al. Dissection of artifactual and confounding glial signatures by single-cell sequencing of mouse and human brain. *Nature neuroscience.* 2022;25(3):306-316.
35. Huang L-H, Lin P-H, Tsai K-W, et al. The effects of storage temperature and duration of blood samples on DNA and RNA qualities. *PloS one.* 2017;12(9):e0184692.
36. Boon BD, Pouwels PJ, Jonkman LE, et al. Can post-mortem MRI be used as a proxy for in-vivo? A case study. *Brain communications.* 2019;
37. Pfefferbaum A, Sullivan EV, Adalsteinsson E, Garrick T, Harper C. Postmortem MR imaging of formalin-fixed human brain. *NeuroImage.* 2004;21(4):1585-1595.
38. Yong-Hing CJ, Obenaus A, Stryker R, Tong K, Sarty GE. Magnetic resonance imaging and mathematical modeling of progressive formalin fixation of the human brain. *Magnetic Resonance in Medicine: An Official Journal of the International Society for Magnetic Resonance in Medicine.* 2005;54(2):324-332.
39. Schmierer K, Wheeler-Kingshott CA, Tozer DJ, et al. Quantitative magnetic resonance of postmortem multiple sclerosis brain before and after fixation. *Magnetic Resonance in Medicine: An Official Journal of the International Society for Magnetic Resonance in Medicine.* 2008;59(2):268-277.
40. Schmierer K, Thavarajah JR, An SF, Brandner S, Miller DH, Tozer DJ. Effects of formalin fixation on magnetic resonance indices in multiple sclerosis cortical gray matter. *Journal of magnetic resonance imaging.* 2010;32(5):1054-1060.
41. Dawe RJ, Bennett DA, Schneider JA, Vasireddi SK, Arfanakis K. Postmortem MRI of human brain hemispheres: T2 relaxation times during formaldehyde fixation. *Magnetic Resonance in Medicine: An Official Journal of the International Society for Magnetic Resonance in Medicine.* 2009;61(4):810-818.
42. Augustinack JC. Postmortem imaging and neuropathologic correlations. *Handbook of clinical neurology.* 2016;136:1321-1339.
43. Tovi M, Ericsson A. Measurements of T1 and T2 over time in formalin-fixed human whole-brain specimens. *Acta Radiologica.* 1992;33(5):400-404.
44. Boyko O, Alston S, Fuller G, Hulette C, Johnson G, Burger P. Utility of postmortem magnetic resonance imaging in clinical neuropathology. *Archives of pathology & laboratory medicine.* 1994;118(3):219-225.

- 1
2
3 45. van Duijn S, Nabuurs RJ, van Rooden S, et al. MRI artifacts in human brain tissue after
4 prolonged formalin storage. *Magnetic resonance in medicine*. 2011;65(6):1750-1758.
5 46. Shepherd TM, Flint JJ, Thelwall PE, et al. Postmortem interval alters the water
6 relaxation and diffusion properties of rat nervous tissue—implications for MRI studies of
7 human autopsy samples. *NeuroImage*. 2009;44(3):820-826.
8 47. Yushkevich PA, Avants BB, Pluta J, et al. A high-resolution computational atlas of the
9 human hippocampus from postmortem magnetic resonance imaging at 9.4 T. *NeuroImage*.
10 2009;44(2):385-398.
11 48. Augustinack JC, Helmer K, Huber KE, Kakunoori S, Zöllei L, Fischl B. Direct
12 visualization of the perforant pathway in the human brain with ex vivo diffusion tensor imaging.
13 *Frontiers in human neuroscience*. 2010:42.
14 49. Adler DH, Liu AY, Pluta J, et al. Reconstruction of the human hippocampus in 3D from
15 histology and high-resolution ex-vivo MRI. *IEEE*; 2012:294-297.
16 50. Adler DH, Pluta J, Kadivar S, et al. Histology-derived volumetric annotation of the
17 human hippocampal subfields in postmortem MRI. *NeuroImage*. 2014;84:505-523.
18 51. Amunts K, Lepage C, Borgeat L, et al. BigBrain: an ultrahigh-resolution 3D human
19 brain model. *Science (New York, NY)*. 2013;340(6139):1472-1475.
20 52. Magnain C, Augustinack JC, Reuter M, et al. Blockface histology with optical
21 coherence tomography: a comparison with Nissl staining. *NeuroImage*. 2014;84:524-533.
22 53. Ceritoglu C, Wang L, Selemon LD, Csernansky JG, Miller MI, Ratnanather JT. Large
23 deformation diffeomorphic metric mapping registration of reconstructed 3D histological section
24 images and in vivo MR images. *Frontiers in human neuroscience*. 2010:43.
25 54. Wachinger C, Navab N. Structural image representation for image registration. *IEEE*;
26 2010:23-30.
27 55. Reuter M, Rosas HD, Fischl B. Highly accurate inverse consistent registration: a robust
28 approach. *NeuroImage*. 2010;53(4):1181-1196.
29 56. Reuter M, Sand P, Huber K. Registration of histology and MRI using blockface as
30 intermediate space. [http://reuter.mit.edu/blue/papers/reuter-hbm12-histo/reuter-hbm12-](http://reuter.mit.edu/blue/papers/reuter-hbm12-histo/reuter-hbm12-histo.pdf)
31 [histo.pdf](http://reuter.mit.edu/blue/papers/reuter-hbm12-histo/reuter-hbm12-histo.pdf).
32 57. Absinta M, Maric D, Gharagozloo M, et al. A lymphocyte–microglia–astrocyte axis in
33 chronic active multiple sclerosis. *Nature*. 2021;597(7878):709-714.
34 58. Glasser MF, Sotiropoulos SN, Wilson JA, et al. The minimal preprocessing pipelines
35 for the Human Connectome Project. *NeuroImage*. 2013;80:105-124.
36
37
38
39
40
41
42
43
44
45
46
47
48
49
50
51
52
53
54
55
56
57
58
59
60

Tables

Table 1: Cases scanned and processed using the Brainbox.

Case No.	Postmortem intervals (Death to scanning)	Age, sex, diagnosis	Premortem MRI available	Fixation times in formaldehyde
1	Unknown*	71, F, multiple brain metastases (primary tumor unknown)	No	> 3 years
2	Unknown*	62, M, subarachnoid bleeding	Yes	> 3 years
3	4 hours	76, M, embolic strokes in several vascular territories caused by aortic dissection	Yes	2 months
4	36 hours	46, M, X-ALD	Yes	2 months
5	12 hours	65, M, COVID-19	Yes	2 months
6	<12 hours	F, Multiple sclerosis	Yes	2 weeks
7	10 hours	14, M, asphyxiation, cavernous hemangioma	No	1 month
8	8 hours	7, F, Unclear enlargement of ventricles with diffuse white matter lesions	No	1 month

Age unknown for the multiple sclerosis patient. * These brains were excluded from the pre- versus post formaldehyde fixation volume analysis because no pre-fixation MRI was available.

Abbreviations: F, female; M, male; MRI, magnetic resonance imaging; X-ALD, X-linked adrenoleukodystrophy.

Figure captions

Figure 1: Brainbox setup

The magnetic resonance imaging (MRI)-compatible Brainbox: exploded (A) and assembled view (B). Titanium screws are used to seal the lid. The Brainbox comprises two main parts: first, a watertight tank (outer compartment, C) with an aperture at the front end, for filling or emptying the tank with medium, e.g., water or formalin. The aperture can either be closed using a lid with vacuum valve for degassing of the specimen (not MRI-compatible) or a standard MRI-compatible lid (D). The second part is an inlet holding the brain (brain holder, inner compartment, E and F). The brain holder can be inserted or removed from the tank with help of a plastic belt with a buckle. This brain holder consists of 16 stackable elements arranged in axial orientation, each with standardized thickness and with an imprinted 3-D coordinate system, identifiable on each individual element (G, with inlet showing a higher magnification). The elements have countable and uniquely identifiable indents in X and Y direction (red arrows) as well as a roman letter in Z direction. The elements also have guiding grooves for facilitating cutting using a brain knife (white arrow).

Abbreviations: MRI, magnetic resonance imaging.

Figure 2: Whole-brain MRI using the Brainbox:

The Brainbox has an imprinted 3D coordinate system with Latin letters in Z direction and unequivocal dots in X and Y direction (A). Whole-brain postmortem MRI from a patient with X-linked adrenoleukodystrophy shows T2w hyperintensities in the deep white matter (B, white arrowheads), similar to the premortem T2w imaging (C). T2w hyperintense, i.e. demarcated stroke in the vascular territory of the middle cerebral artery affecting the basal ganglia, the internal capsule and the insula, in fresh (D, white arrowheads) and after 3 weeks of formaldehyde fixation (E), similar to the diffusion restriction in premortem MRI (F). Also smaller imaging features such as enlarged perivascular spaces in the basal ganglia (G and J, premortem T1w image) or a lacunar stroke (H and K, premortem T1w scan) are conspicuous using our high-resolution MRI protocol of the whole human brain in the Brainbox (inlets with higher magnification). Brains which were fixed for 2 - 3 weeks show volume decrease (inlets with higher magnification of the temporal region) (I and L).

Abbreviations: MRI, magnetic resonance imaging; T1w, T1-weighted; T2; T2-weighted.

Figure 3: High-resolution brain MRI from a COVID-19 donor using the Brainbox.

High-resolution magnetic resonance imaging (MRI) of a brain from a COVID-19 donor, employing gradient echo magnetization transfer imaging (A and C) and gradient echo quantitative susceptibility mapping (B and D). Nominal resolution: 0.4 mm isotropic.

Figure 4: Imaging to histopathology correlation using the Brainbox.

The Brainbox can facilitate correlation of magnetic resonance imaging (MRI) features to histopathology. A: A volume of interest is identified on the MR image, e.g., a hypointense ovoid lesion in the right internal capsule, corresponding to either an enlarged perivascular space (EPVS) or a lacunar stroke (white circle). The 3D coordinate system is used to identify its location in relation to the Brainbox (red lines and red circle). B: Identification of the lesion in the macroscopic view in the brain using the coordinate system (white rectangle labelling volume of interest, close-up in the top right corner). C: Cutting a tissue block. D: Histopathological work-up using H&E staining and showing a tissue defect, consistent with a chronic lacunar stroke (scale bar: 2 mm). E-G: Unclear haemorrhagic lesion in the right angular gyrus (white arrow). Note the ribbon-shaped artifact at the grey-white matter junction can stem from relatively short brain fixation in formaldehyde. H: This unclear lesion was correlated to its tissue substrate using the Brainbox (scale bar: 2 cm). I: Histopathology using H&E staining reveals a cavernous hemangioma with abnormal blood vessels (black arrow, scale bar: 2 mm). J: Elastica van Gieson (EvG) stain highlights cavernous dilatations and thickened wall in places (inset, scale bar: 250 μ m) K: Iron staining using Prussian blue demonstrates hemosiderin in perilesional old microhaemorrhages (scale bar: 250 μ m). L and M: Immunohistochemistry demonstrates fibrillary GFAP-positive astrogliosis (L) and CD68 in reactive microglia (M) (scale bar: A: 2cm, I-M 2mm, insets: 250 μ m).

Abbreviations: EvG, Elastica van Gieson; GFAP, glial fibrillary acidic protein; H&E, hematoxylin and eosin; MRI, magnetic resonance imaging.

Figure 5: Pipeline for MRI-histopathology correlation using the Brainbox.

1
2
3
4
5
6
7
8
9
10
11
12
13
14
15
16
17
18
19
20
21
22
23
24
25
26
27
28
29
30
31
32
33
34
35
36
37
38
39
40
41
42
43
44
45
46
47
48
49
50
51
52
53
54
55
56
57
58
59
60

1: The brain is retrieved upon autopsy and mounted in the brain holder (inner compartment) of the Brainbox; 2: The brain holder is inserted into the tank filled with an aqueous medium, e.g., water or phosphate-buffered saline (PBS); 3: First magnetic resonance imaging (MRI) scan of the brain using a 20-channel head coil; 4: Replace aqueous medium with fixative solution, e.g., 10% neutral-buffered formalin. Of note, the medium can be changed by pouring out the medium and filling the tank with another medium, i.e., the brain position within the brain holder remains unchanged. The brain can be soaked/stored until acquisition of next MRI; 5: Second MRI scan; 6: Identification of a volume of interest (VOI) within the MR images, e.g., a presumable lacunar stroke. Reference points for later tissue retrieval can be identified on the built-in 3D coordinate system ;7: Axial/transversal sectioning of the brain according to the identified coordinates; 8: Retrieval of tissue block of interest; 9: Histo(patho)logical processing of tissue block, .e.g., embedding in paraffin.

Abbreviations: MRI, magnetic resonance imaging; PBS, phosphate-buffered saline; VOI, volume of interest.

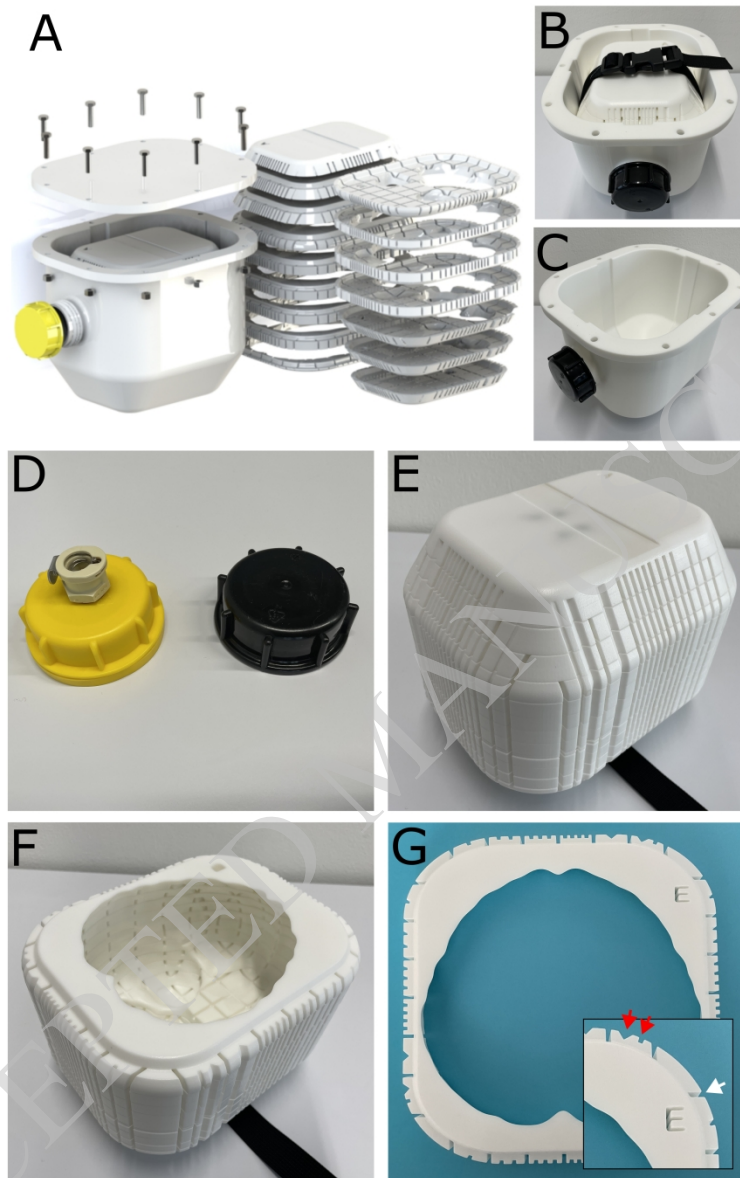


Figure 1: Brainbox setup

The magnetic resonance imaging (MRI)-compatible Brainbox: exploded (A) and assembled view (B). Titanium screws are used to seal the lid. The Brainbox comprises two main parts: first, a watertight tank (outer compartment, C) with an aperture at the front end, for filling or emptying the tank with medium, e.g., water or formalin. The aperture can either be closed using a lid with vacuum valve for degassing of the specimen (not MRI-compatible) or a standard MRI-compatible lid (D). The second part is an inlet holding the brain (brain holder, inner compartment, E and F). The brain holder can be inserted or removed from the tank with help of a plastic belt with a buckle. This brain holder consists of 16 stackable elements arranged in axial orientation, each with standardized thickness and with an imprinted 3-D coordinate system, identifiable on each individual element (G, with inset showing a higher magnification). The elements have countable and uniquely identifiable indents in X and Y direction (red arrows) as well as a roman letter in Z direction. The elements also have guiding grooves for facilitating cutting using a brain knife (white arrow). Abbreviations: MRI, magnetic resonance imaging.

417x649mm (236 x 236 DPI)

ACCEPTED MANUSCRIPT

1
2
3
4
5
6
7
8
9
10
11
12
13
14
15
16
17
18
19
20
21
22
23
24
25
26
27
28
29
30
31
32
33
34
35
36
37
38
39
40
41
42
43
44
45
46
47
48
49
50
51
52
53
54
55
56
57
58
59
60

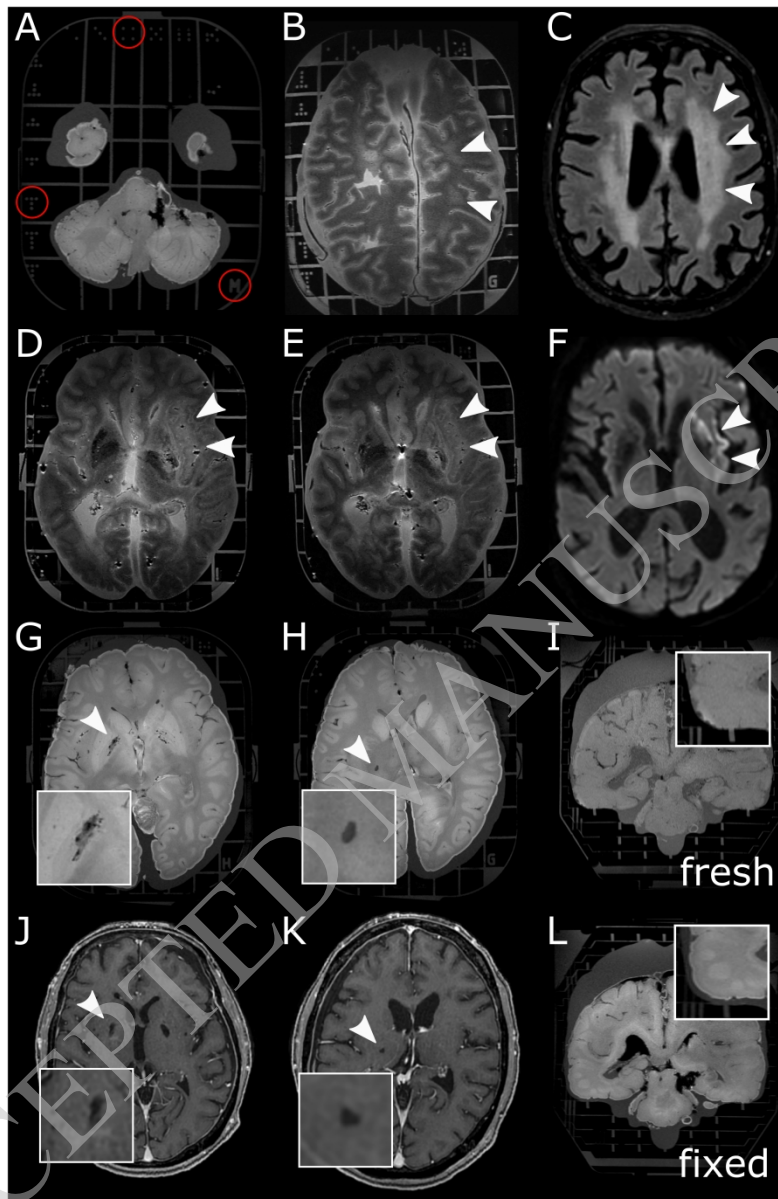


Figure 2: Whole-brain MRI using the Brainbox:

The Brainbox has an imprinted 3D coordinate system with Latin letters in Z direction and unequivocal dots in X and Y direction (A). Whole-brain postmortem MRI from a patient with X-linked adrenoleukodystrophy shows T2w hyperintensities in the deep white matter (B, white arrowheads), similar to the premortem T2w imaging (C). T2w hyperintense, i.e. demarcated stroke in the vascular territory of the middle cerebral artery affecting the basal ganglia, the internal capsule and the insula, in fresh (D, white arrowheads) and after 3 weeks of formaldehyde fixation (E), similar to the diffusion restriction in premortem MRI (F). Also smaller imaging features such as enlarged perivascular spaces in the basal ganglia (G and J, premortem T1w image) or a lacunar stroke (H and K, premortem T1w scan) are conspicuous using our high-resolution MRI protocol of the whole human brain in the Brainbox (inlets with higher magnification). Brains which were fixed for 2 - 3 weeks show volume decrease (inlets with higher magnification of the temporal region) (I and L).

Abbreviations: MRI, magnetic resonance imaging; T1w, T1-weighted; T2; T2-weighted.

446x679mm (236 x 236 DPI)

ACCEPTED MANUSCRIPT

1
2
3
4
5
6
7
8
9
10
11
12
13
14
15
16
17
18
19
20
21
22
23
24
25
26
27
28
29
30
31
32
33
34
35
36
37
38
39
40
41
42
43
44
45
46
47
48
49
50
51
52
53
54
55
56
57
58
59
60

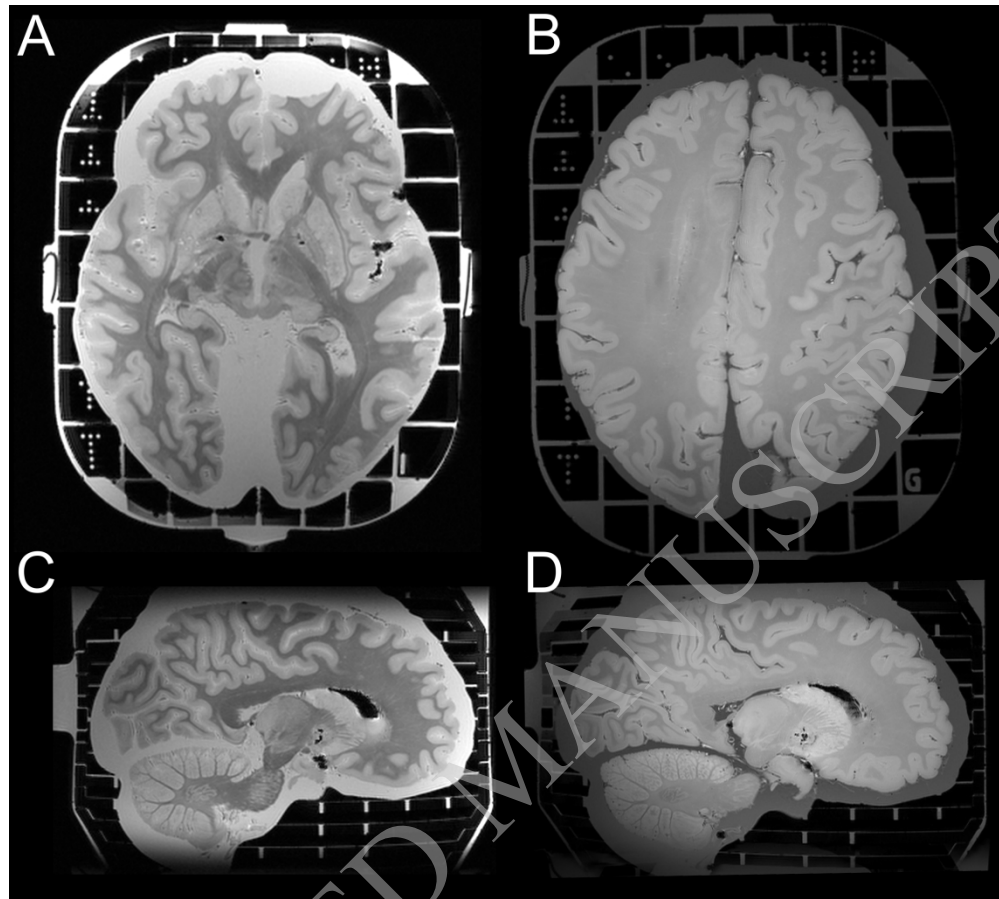


Figure 3: High-resolution brain MRI from a COVID-19 donor using the Brainbox. High-resolution magnetic resonance imaging (MRI) of a brain from a COVID-19 donor, employing gradient echo magnetization transfer imaging (A and C) and gradient echo quantitative susceptibility mapping (B and D). Nominal resolution: 0.4 mm isotropic.

476x426mm (236 x 236 DPI)

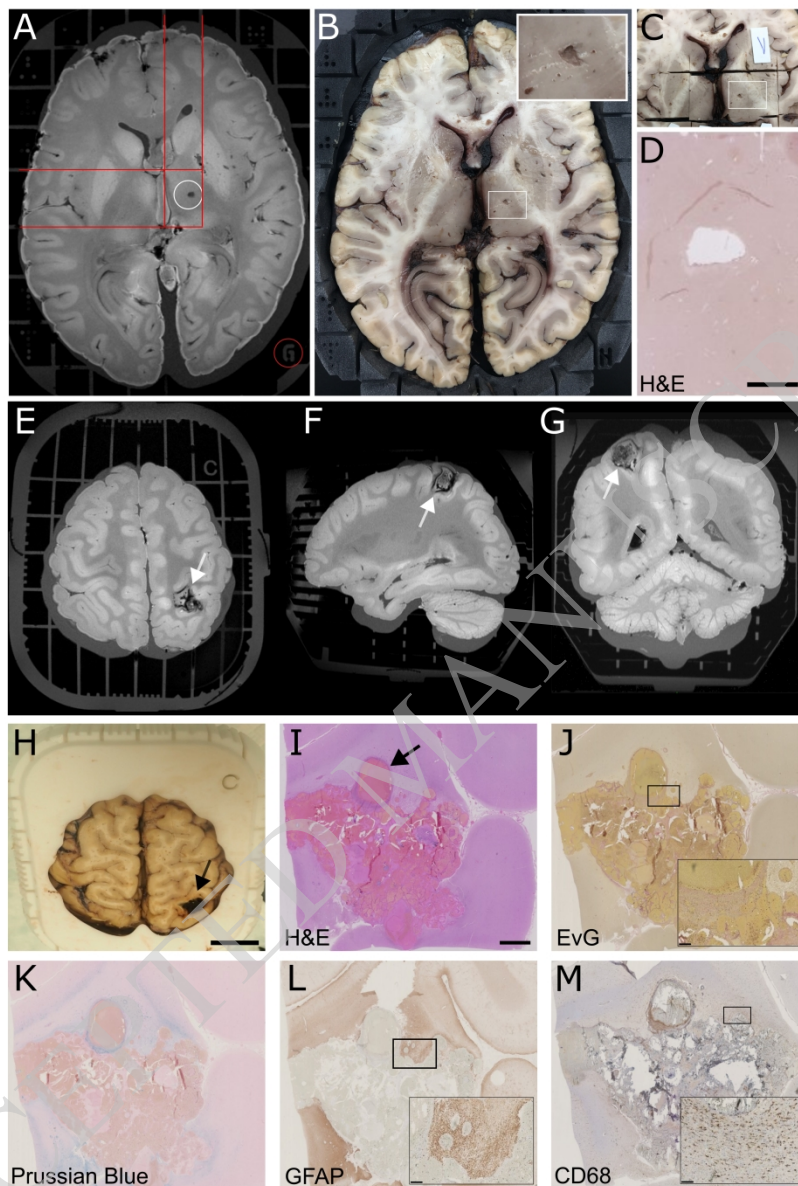


Figure 4: Imaging to histopathology correlation using the Brainbox.

The Brainbox can facilitate correlation of magnetic resonance imaging (MRI) features to histopathology. A: A volume of interest is identified on the MR image, e.g., a hypointense ovoid lesion in the right internal capsule, corresponding to either an enlarged perivascular space (EPVS) or a lacunar stroke (white circle). The 3D coordinate system is used to identify its location in relation to the Brainbox (red lines and red circle).

B: Identification of the lesion in the macroscopic view in the brain using the coordinate system (white rectangle labelling volume of interest, close-up in the top right corner). C: Cutting a tissue block. D: Histopathological work-up using H&E staining and showing a tissue defect, consistent with a chronic lacunar stroke (scale bar: 2 mm). E-G: Unclear haemorrhagic lesion in the right angular gyrus (white arrow). Note the ribbon-shaped artifact at the grey-white matter junction can stem from relatively short brain fixation in formaldehyde. H: This unclear lesion was correlated to its tissue substrate using the Brainbox (scale bar: 2 cm). I: Histopathology using H&E staining reveals a cavernous hemangioma with abnormal blood vessels (black arrow, scale bar: 2 mm). J: Elastica van Gieson (EvG) stain highlights cavernous dilatations and thickened wall in places (inset, scale bar: 250 μ m). K: Iron staining using Prussian blue demonstrates

1
2
3 hemosiderin in perilesional old microhaemorrhages (scale bar: 250 μ m). L and M: Immunohistochemistry
4 demonstrates fibrillary GFAP-positive astrogliosis (L) and CD68 in reactive microglia (M) (scale bar: A: 2cm,
5 I-M 2mm, insets: 250 μ m).

6 Abbreviations: EvG, Elastica van Gieson; GFAP, glial fibrillary acidic protein; H&E, hematoxylin and eosin;
7 MRI, magnetic resonance imaging.

8 464x672mm (236 x 236 DPI)
9
10
11
12
13
14
15
16
17
18
19
20
21
22
23
24
25
26
27
28
29
30
31
32
33
34
35
36
37
38
39
40
41
42
43
44
45
46
47
48
49
50
51
52
53
54
55
56
57
58
59
60

ACCEPTED MANUSCRIPT

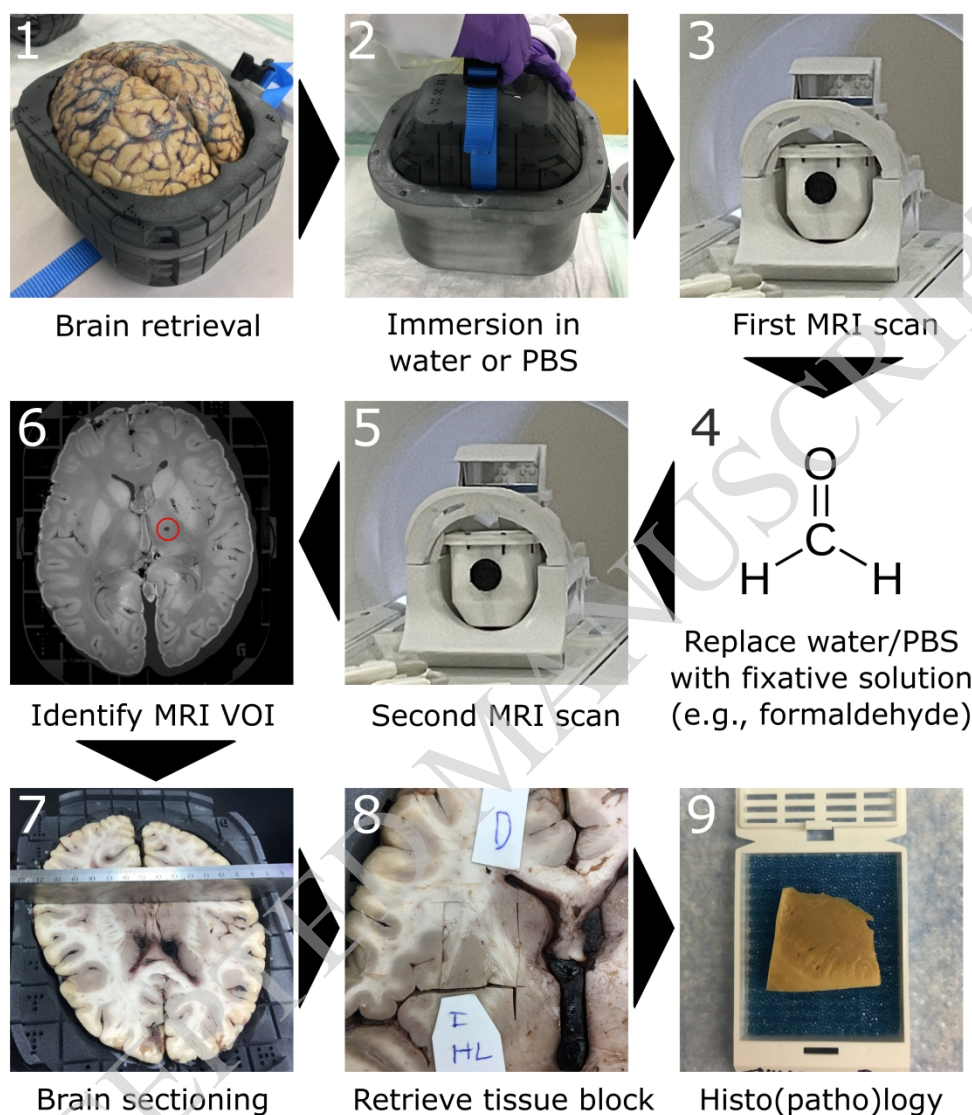


Figure 5: Pipeline for MRI-histopathology correlation using the Brainbox.

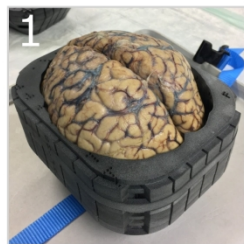
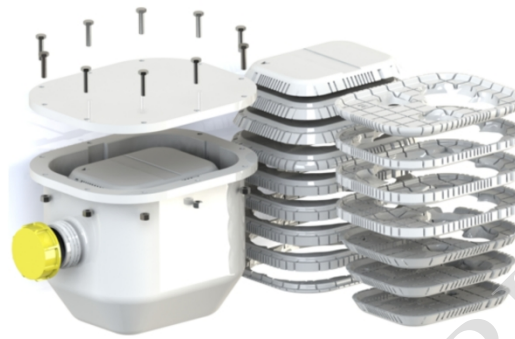
1: The brain is retrieved upon autopsy and mounted in the brain holder (inner compartment) of the Brainbox; 2: The brain holder is inserted into the tank filled with an aqueous medium, e.g., water or phosphate-buffered saline (PBS); 3: First magnetic resonance imaging (MRI) scan of the brain using a 20-channel head coil; 4: Replace aqueous medium with fixative solution, e.g., 10% neutral-buffered formalin. Of note, the medium can be changed by pouring out the medium and filling the tank with another medium, i.e., the brain position within the brain holder remains unchanged. The brain can be soaked/stored until acquisition of next MRI; 5: Second MRI scan; 6: Identification of a volume of interest (VOI) within the MR images, e.g., a presumable lacunar stroke. Reference points for later tissue retrieval can be identified on the built-in 3D coordinate system; 7: Axial/transversal sectioning of the brain according to the identified coordinates; 8: Retrieval of tissue block of interest; 9: Histo(patho)logical processing of tissue block, .e.g., embedding in paraffin.

Abbreviations: MRI, magnetic resonance imaging; PBS, phosphate-buffered saline; VOI, volume of interest.

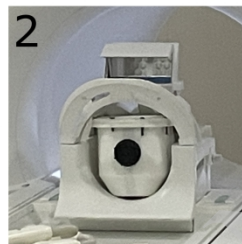
493x559mm (236 x 236 DPI)

Brainbox

MRI-compatible brain container with 3D coordinate system to correlate MRI features to histopathology



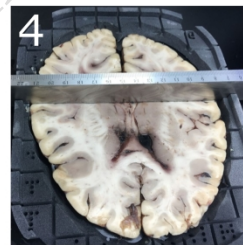
1
Brain retrieval upon autopsy



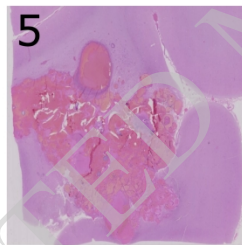
2
Magnetic resonance imaging (MRI)



3
Identify volume of interest



4
Brain sectioning



5
Histopathology

Graphical abstract

416x437mm (236 x 236 DPI)

ACCEPTED MANUSCRIPT

1
2
3
4
5
6
7
8
9
10
11
12
13
14
15
16
17
18
19
20
21
22
23
24
25
26
27
28
29
30
31
32
33
34
35
36
37
38
39
40
41
42
43
44
45
46
47
48
49
50
51
52
53
54
55
56
57
58
59
60